frontiers | Frontiers in Physics

TYPE Original Research
PUBLISHED 25 November 2025
DOI 10.3389/fphy.2025.1688864

OPEN ACCESS

EDITED BY
Chong Qi,
Royal Institute of Technology, Sweden

REVIEWED BY
Danyang Pang,
Beihang University, China
Ruirui Xu,
China Institute of Atomic Energy, China

*CORRESPONDENCE
A. S. Tkachenko,
tkachenko.alessya@gmail.com

RECEIVED 19 August 2025
REVISED 26 September 2025
ACCEPTED 30 September 2025
PUBLISHED 25 November 2025

CITATION
Tkachenko AS, Burkova NA, Yeleusheva BM and Dubovichenko SB (2025) Estimation of the effect of Tsallis non-extensive statistics on the $^{14}C(n,\gamma)^{15}C$ reaction rate.
Front. Phys. 13:1688864.
doi: 10.3389/fphy.2025.1688864

Estimation of the effect of Tsallis non-extensive statistics on the $^{14}C(n,\gamma)^{15}C$ reaction rate

A. S. Tkachenko *[1], N. A. Burkova [2], B. M. Yeleusheva [1] and S. B. Dubovichenko [1]

[1]Department of Science, Eurasian Technological University, Almaty, Kazakhstan, [2]Faculty of Physics and Technology, Al-Farabi Kazakh National University, Almaty, Kazakhstan

The total cross-section of the radiative neutron capture reaction $^{14}C(n,\gamma_{0+1})^{15}C$—for energies ranging from 10 meV to 5 MeV—is considered. Calculations performed in the framework of the modified potential cluster model with forbidden states show an agreement of total cross-section σ (23.3 keV) = 4.75 μb with the presently recommended value 4.86(48) μb by Ma et al., 2020. The efficiency of carbon isotope ^{15}C production is illustrated by the $^{14}C(n,\gamma_{0+1})^{15}C$ reaction rate calculated at temperatures from T_9 = 0.001 to T_9 = 10. The conventional Maxwell–Boltzmann weighted reaction rate $\langle\sigma v\rangle_{MB}$ of the present work is comparable, with less than 10% accuracy, with the latest calculations by Ma et al., 2020 and Bhattacharyya et al., 2021. The estimation of non-extensive effects is implemented using our data on the reaction rate $\langle\sigma v\rangle_{MB}$ as reference values. The efficiency of carbon isotope production in radiative capture reactions $^{12\text{-}14}C(n,\gamma)^{13\text{-}15}C$ is estimated based on the calculated reaction rates. The influence of the Maxwellian-weighted $^{12\text{-}14}C(n,\gamma)^{13\text{-}15}C$ reaction rates on the ratios $^{12}C/^{13}C$ and $^{13}C/^{14}C$ is examined. Tsallis statistics is applied for the first time to the calculation of the $^{14}C(n,\gamma_0)^{15}C$ reaction rate with values of non-extensive parameter $0.7 \leq q \leq 1.3$ on the background of Maxwell–Boltzmann statistics corresponding to q = 1. The reaction rate $\langle\sigma v\rangle_q$ shows a factor ~4 increase for q = 0.7 and a factor ~0.6 decrease for q = 1.3 compared to q = 1.

KEYWORDS

n^{14}C system, radiative capture, thermonuclear reaction rate, potential cluster model, Tsallis statistics

1 Introduction

The role of carbon isotope ^{14}C in the stellar environment of asymptotic giant branch (AGB) stars was examined nearly 30 years ago by Forestini and Charbonnel, 1997, as part of research concerning the nucleosynthesis of light elements in low-metallicity intermediate-mass stars of $3-7M_{\odot}$ [1, 2]. We found it very interesting how the authors incorporated the isotope ^{14}C into the scenario of AGB star evolution as some of their perspectives can now be validated with contemporary data. To reconstruct the AGB evolution, the network of neutron-, proton-, and ^{4}He-induced reactions was considered on some selected nuclides, particularly $^{14}C(n,\gamma)$, $^{14}C(p,\gamma)$, $^{14}C(\alpha,\gamma)$, and $^{14}C(\alpha,n)$ processes, with ^{14}C as the seed nucleus [1, 2]. The production of ^{14}C is provided by two reactions: $^{13}C(n,\gamma)^{14}C$ and $^{14}N(n,p)^{14}C$, so it is important to briefly discuss the status of these processes today.

The results of [1] are presented as an estimation of isotope abundance in carbon pockets:

$$^{12}C/^{13}C = 44 \pm 3, ^{13}C/^{14}C > 1400, ^{14}N/^{15}N > 5300. \quad (1)$$

These numbers turned out to be reference values, to some extent, for subsequent studies of AGB stars. Some original papers and reviews provide observables for the $^{12}C/^{13}C$ and $^{14}N/^{15}N$ ratios in AGB stars [3–6]. Note that ratios in Equation 1 strongly depend on the mutually connected reaction chains, such as neutron-induced reactions

$$^{12}C(n,\gamma)^{13}C(n,\gamma)^{14}C(n,\gamma)^{12}C(\beta^-)^{15}N, \quad (2)$$

where the evolution of carbon isotopes $^{12\text{-}15}C$ occurs, and finally nitrogen ^{15}N is created. Hydrogen burning, $^{12\text{-}14}C(p,\gamma)^{13\text{-}15}N$, is the source of nitrogen isotopes, providing the $^{14}N/^{15}N$ ratio while also regulating the carbon fractions. We are not concerned with the mechanism of ^4He combustion since it mainly relates to the outer helium shell of AGB stars, which is beyond the scope of the present work.

We intend to discuss [5], purposely, the situation with the radiative neutron capture reaction $^{14}C(n,\gamma)^{15}C$ in the context of the following questions:

1. i. how reliable is the reaction rate determined today?;
2. ii. how may modern data on the reaction rate change the isotopic ratio (Equation 1)?;
3. iii. are there any reasons to shift from the traditional Maxwell–Boltzmann (MB) weighted reaction rate to non-extensive statistics?

While calculating the ratios (Equation 1), Forestini and Charbonnel, 1997 [1], used as input information for the constructed network the rate of the $^{14}C(n,\gamma)^{15}C$ reaction obtained in [7], which was nearly a factor of 5 lower than that of the earlier calculations in [8]. As a result, it was concluded that the reaction $^{14}C(n,\gamma)^{15}C(\beta^-)^{15}N$ plays an insignificant role in the formation of ^{15}N, with the process of radiative capture of protons $^{14}C(p,\gamma)^{15}N$ dominating.

This "factor of 5 difference" triggered, to some extent, the following year's experimental study of the cross section of $^{14}C(n,\gamma)^{15}C$ reaction [9–12]. The value of the total cross section $\sigma(E)$ at $E_{c.m.} = 23.3$ keV is a benchmark today for comparing experimental methods and theoretical models. We suggest, for analysis, the set of results for $\sigma(23.3\ \text{keV})$ from [7, 9, 11–19, 49] and the recently published data by [20].

To determine the consistency of the results on the MB-weighted rate of the $^{14}C(n,\gamma)^{15}C$ reaction, we use data from [7, 8, 11, 18, 19] along with the present model calculations to address question (i). Since we employed the modified potential cluster model (MPCM) (see, for details, [21, 22]), the comparison of rates for the neutron-induced reactions $^{12\text{-}14}C(n,\gamma)^{13\text{-}15}C$ calculated within the same framework provides a way to re-estimate the $^{13}C/^{14}C$ ratio (ii).

Question (iii) is a new issue in the study of the $^{14}C(n,\gamma)^{15}C$ reaction. The subject of non-equilibrium phenomena in the context of stars is related to the application of non-extensive Tsallis statistics, as suggested in [23]. For the first time, [24] (final version, 2017 [25]), pointed out the strong sensitivity of thermonuclear reaction rates of light nuclei during Big Bang nucleosynthesis to the non-extensive parameter q. Further investigations concern the effect of Tsallis statistics on primordial BBN in the context of addressing the lithium problem [26, 27]. A summary of the research [24, 25] suggested extending the study of non-extensive effects to the formation of nuclei with masses beyond the BB seeds, i.e., with $A > 7$. The authors foresee a possible new comprehension of the synthesis of heavy elements. In the present work, we applied the formalism of Tsallis statistics [24, 25] to illustrate its effect on the $^{14}C(n,\gamma)^{15}C$ reaction rate.

2 Elements of MPCM input data for the $^{14}C(n,\gamma_{0+1})^{15}C$ reaction

The details of the study of the $^{14}C(n,\gamma_{0+1})^{15}C$ reaction in the framework of the MPCM are presented in [28]. In this study, we still consider radiative $E1$ neutron capture on ^{14}C, scattering p-waves to the ground state (GS) and first excited state (1^{st} ES) of ^{15}C, with respective quantum numbers $^2P_{1/2}+^2P_{3/2}\rightarrow^2S_{1/2}$ and $^2P_{3/2}\rightarrow^2D_{5/2}$. The interaction potential used for the calculation of continuum and bound states is of the Gauss type

$$V(r,JLS) = -V_0(JLS)\exp\{-\alpha(JLS)r^2\}, \quad (3)$$

where V_0 is the potential depth and α is a parameter defining the asymptotic decrease in the potential at long relative distances r. Parameters V_0 and α in Equation 3 are fitted for the bound states so that they match the channel binding energy E_b, charge radius R_{ch}, and matter radius R_m. A set of parameters is found for each partial wave with quantum numbers JLS. The nodal or nodeless r-dependence of the relative wave functions is determined by the classification of orbital symmetry using Young diagrams, as implemented for the $n+^{14}C$ system in [28].

Another experimental characteristic is the asymptotic normalization coefficient A_{NC} (ANC), which is related to the dimensional asymptotic constant C via the spectroscopic factor S_F as follows: $A^2_{NC} = S_F \times C^2$ [29]. We work in the formalism of the dimensionless asymptotic constant C_w, which is related to C by $C_w = C/\sqrt{2k_o}$, where the wave number k_0 corresponds to the channel binding energy $E_b = \hbar^2 k_o^2/2\mu$ and μ is the reduced mass. The asymptotic constant C_w is determined by matching the numerical radial function to the analytical Whittaker function: $\chi_L(r) = \sqrt{2k_0}C_w W_{-\eta L+1/2}(2k_0 r)$. In the case of neutron-induced reactions, $\eta = 0$. The corresponding results are provided in Table 1.

To calculate $R_{ch}(^{15}C)$ and $R_m(^{15}C)$, we follow the definitions from [21]. The input numerical information includes the masses of the constituent particles, $m_n = 1.008665$ amu and $m_{^{14}C} = 14.003242$ amu; the averaged value of $R_{ch}(^{14}C) = 2.48$ fm from [30–32]; and the latest data for $R_m(^{14}C) = 2.367(35)$ fm from[33]. The recent experimental data on the ground state charge R_{ch} and matter radius R_m for ^{15}C, presented in Table 2, show good agreement with the MPCM results (see Table 1).

The results for C_w in Table 1 were obtained over the interval 7–27 fm. Selected later data on the ANC and their recalculated values for C_w, presented in Table 3, show reasonable agreement with the MPCM results for the GS, as well as for the first excited state.

Initially, we proceeded from the data in work [37], where for the resonant states $^2P_{1/2}$ at 3.103 MeV and $^2P_{3/2}$ at 4.657 MeV, the reaction $^{14}C(n,\gamma)^{15}C$ does not occur, which means that these states are excited or formed in stripping or pickup reactions. In

TABLE 1 Parameters of the ground and excited state potential for ^{15}C nucleus in the n^{14}C channel and results of MPCM calculations of E_b, R_{ch}, R_m, and C_w with the listed parameters V_0 and α.

Set	V_0, MeV	α, fm^{-2}	E_b, MeV	R_{ch} (^{15}C), fm	R_m (^{15}C), fm	C_w
GS ($^2S_{1/2}$)	93.581266	0.2	1.21809	2.52	2.60	1.84(1)
ES ($^2D_{5/2}$)	256.981908	0.2	0.4781	2.51	2.53	0.13(1)

TABLE 2 Data on the experimentally measured charge radius R_{ch} and matter radius R_m of ^{15}C.

Reference	R_{ch} (^{15}C), fm	Reference	R_m (^{15}C), fm
Yamaguchi et al. [30]	2.47(8)	Kanungo et al. [34]	2.54(4)
Zhao et al. [32]	2.56(27)	Dobrovolsky et al. [35]	2.59 (5)
Zhao et al. [31]	2.56(20)	Li et al. [33]	2.509(40)

TABLE 3 Asymptotic constant data for ^{15}C in the n^{14}C channel.

Reference	ANC, fm$^{-1/2}$	S_f	C_w
GS			
McCleskey et al., [15]	1.37(7)	1	2.00(10)
Moschini et al. [17]	1.26(2)	1	1.84(3)
Ma et al. [18]	1.34(7)	0.82(7)	2.17(21)
Hebborn and Capel [36]	1.25(12)	1	1.82(18)
Jiang et al. [20]	1.16(15)	0.68(14)	2.10(42)
1st ES			
Mukhamedzhanov et al. [49]	0.0595(36)	1	0.105(6)
McCleskey et al. [15]	0.0653(14)	1	0.115(2)

some studies, the narrow resonance at 3.103 MeV (Γ_n = 42 keV) is included in ^{14}C$(n,\gamma)^{15}$C cross-section calculations as a Breit–Wigner resonance; for example, see recent references [18, 20]. Their estimates show that its contribution is very small, even compared to the capture to the first excited state.

In the present study, we assume the $^2P_{1/2}$ and $^2P_{3/2}$ states to be non-resonant in the n + ^{14}C channel. Since in the MPCM, the partial ^2P waves do not contain forbidden states [22, 28], which are present in the spectrum of solutions of the Schrödinger equation only as bound states and require sufficiently deep attractive potentials [21], we assume the corresponding potentials to be zero.

Our choice of the zero depth for the P-wave scattering interaction potentials is supported by Ref. [16], where the role of different interaction parameters sets in the continuum n+^{14}C channel is examined for the Coulomb breakup of ^{15}C, and from these data the radiative capture ^{14}C$(n,\gamma_0)^{15}$C cross sections are recalculated.

3 Total cross sections of the n^{14}C capture reaction

Comparison of the total cross sections for the ^{14}C$(n,\gamma_{0+1})^{15}$C reaction, calculated using the MPCM potential parameters from Table 1, with experimental data is presented in Figure 1a. It is clearly observed that there is a noticeable input from the (n,γ_1) capture to the first ES starting from energies $E_{c.m.} \sim 1$ MeV.

Note that the data by [12] are the result of a recalculation of the Coulomb breakup of ^{15}C and corresponds to the photodisintegration reaction ^{15}C$(\bar{\gamma},n)^{14}$C by virtual photons. When compared to direct photodisintegration by real γ-quanta, the results may differ. In general, it should be acknowledged that the measurement errors are very large, and all experimental points refer to the GS radiative capture ^{14}C$(n,\gamma_0)^{15}$C process.

Figure 1b illustrates the total cross sections for $E_{c.m.}$ shows the results from our earlier work [28]. These cross sections are somewhat lower than the present cross sections since in [28], the radial matrix elements for the cross sections were calculated only up to 30 fm. Based on the low binding energy E_b of the n^{14}C system, we have extended the integration interval for the overlapping integrals up to a distance of 100 fm.

The energy dependence of $\sigma(E_{c.m.})$ at $E_{c.m.} \leq 10$ keV (red solid curve in Figure 1b) can be approximated by the simple functional form:

$$\sigma_{ap}(\mu b) = A\sqrt{E_{c.m.}(keV)}. \quad (4)$$

The constant A = 1.002 μb·keV$^{-1/2}$ in equation 4 is determined from a single point of $\sigma(E_{c.m.})$ at the minimum energy of 10 MeV. The value $A = 0.782\,\mu b \cdot keV^{-1/2}$ obtained earlier in [28] is approximately 20% lower. The accuracy of approximation (Equation 4) is estimated as $M(E) = \left|\left[\sigma_{ap}(E) - \sigma_{theor}(E)\right]/\sigma_{theor}(E)\right|$. The relative deviation of the calculated theoretical cross section $\sigma_{theor}(E)$ and its approximation $\sigma_{ap}(E)$ by the above function at energies less than 10 keV does not exceed 0.8%. Relation (Equation 4) allows determining the value of the thermal cross section: σ_{th}(25.3 meV) ≃ 0.005 μb.

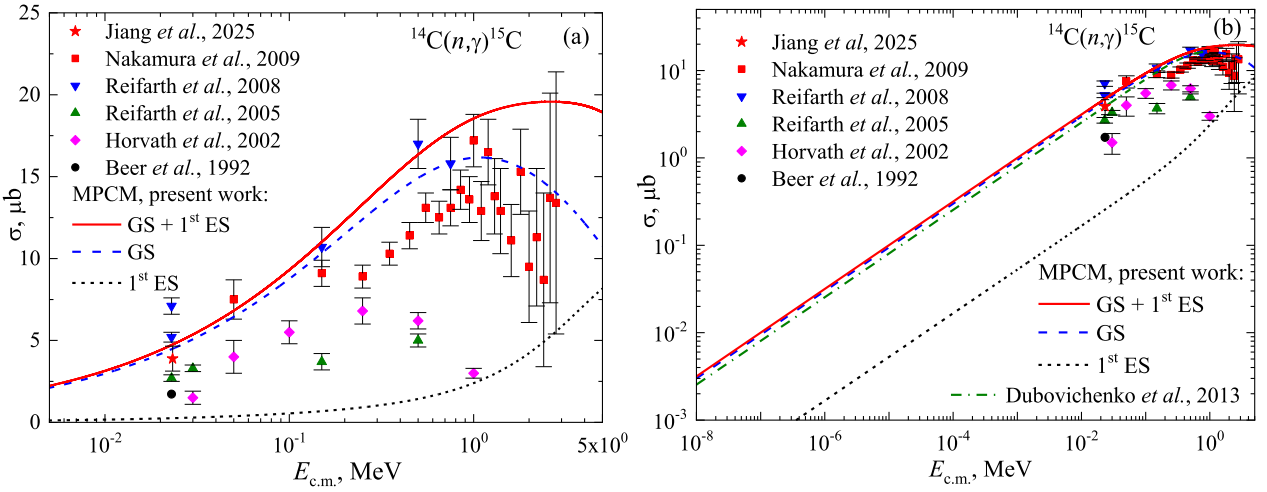

FIGURE 1
Total cross sections of the $^{14}C(n,\gamma_{0+1})^{15}C$ reaction. Experiment: ★, [20]; ■, [12]; ▼, [11]; ▲, [10]; ◆, [9]; ●, [7]. Curves: MPCM calculations. **(a)** $E_{c.m.}$ = 5 keV–5 MeV. **(b)** $E_{c.m.}$ = 10^{-8}–5 MeV; green dash-dotted curve–results of [28].

The thermal cross section is too small to be measured; therefore, the available experimental value of $\sigma(E_{c.m.})$ at $E_{c.m.}$ = 23.3 keV is a benchmark for comparing different experimental methods and the results obtained from various theoretical models. The summary at σ(23.3keV) is presented in Table 4. We note the good agreement of our calculations with the data of [16], [18], [19], and with the evaluated values suggested as the presently recommended values.

Figure 2 shows the neutron capture cross section divided by $E^{1/2}$, i.e., $S_n(E) = \sigma(E)/\sqrt{E}$. It should be noted that the theoretical calculations [13, 18] and the present MPCM results agree well. At an energy of 10^{-8} MeV, $S_n(E)$ = 1.002 μb·keV$^{-1/2}$ for the total cross section and $S_n(E)$ = 0.949 μb·keV$^{-1/2}$ for capture to the GS, corresponding to ~95% dominance. The contribution of the first ES is ~5% at low energies.

4 $^{14}C(n,\gamma_{0+1})^{15}C$ reaction rate

The astrophysical rate of the $^{14}C(n,\gamma_{0+1})^{15}C$ reaction, calculated in MPCM, is shown in Figure 3. We approximated the MPCM reaction rates using an expression of the form ($T_9 = 10^9$K):

$$N_A\langle\sigma v\rangle = a_1/T_9^{2/3}\exp\left(-a_2/T_9^{1/3}\right)\left(1.0 + a_3T_9^{1/3} + a_4T_9^{2/3} + a_5T_9 + a_6T_9^{4/3} + a_7T_9^{5/3}\right) + a_8T_9^{a_9}. \quad (5)$$

Corresponding parameters a_i for the GS and total reaction rates are provided in Table 5 according (Equation 5). The approximation yields χ^2 = 0.0005 and χ^2 = 0.0006, respectively, with an accuracy of 5% for the calculated reaction rates.

The inset in Figure 3 shows a comparison of present results and reaction rates calculated by [11], [18], and [19] normalized to the rate of the present work. The rate [18] based on the ANC formalism in the interval T_9 = 0.003 – 5 shows agreement with the MPCM rate within +5% on average, which is very close to that of [11]. The reaction rate in [19] derived from the Coulomb dissociation data is near ~10% lower than the MPCM rate at the temperatures of T_9 = 0.01 – 1. In summary, the results of the MPCM are in very good agreement with the modern data from [18, 19].

TABLE 4 Comparison of the ^{14}C neutron capture cross sections at $E_{c.m.}$ = 23.3 keV.

Reference	σ, μb
Beer et.al. [7]	1.72(43) [a]
Horvath et al. [9]	2.6(9)
Timofeyuk et al. [13]	5.3(3) [b]
Reifarth et al. [11]	5.2(3) or 7.1(5) [b]
Summers and Nunes [14]	7.1(5)
Nakamura et al. [12]	6.1(5) [a]
McCleskey et al. [15]	5.4(5)
Capel and Nollet [16]	4.74(27)
Moschini et al. [17]	5.8(2)
Ma et al. [18]	4.97(42)
Ma et al. [18]	4.86(48) [c]
Bhattacharyya et al. [19]	4.4(3)
Jiang et al. [20]	3.89(76)
Present work	4.75

[a]Maxwellian-averaged cross section at kT = 23.3 keV
[b]Cross section at a neutron energy E_n = 23.3 keV
[c]Presently recommended value.

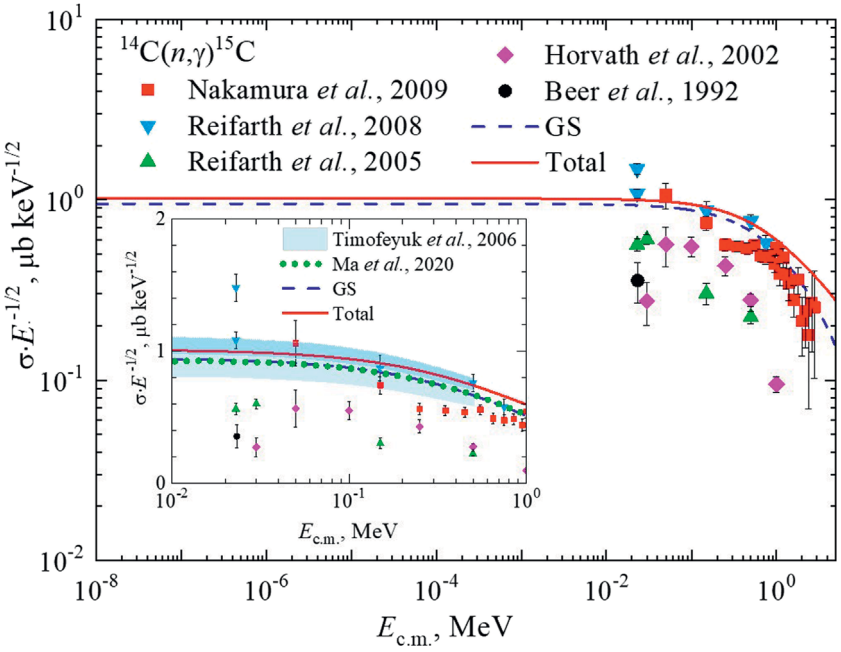

FIGURE 2
Total cross sections of the radiative n^{14}C capture divided by $E^{1/2}$. The inset shows the comparison of the theoretical calculations of [13, 18] and the MPCM results.

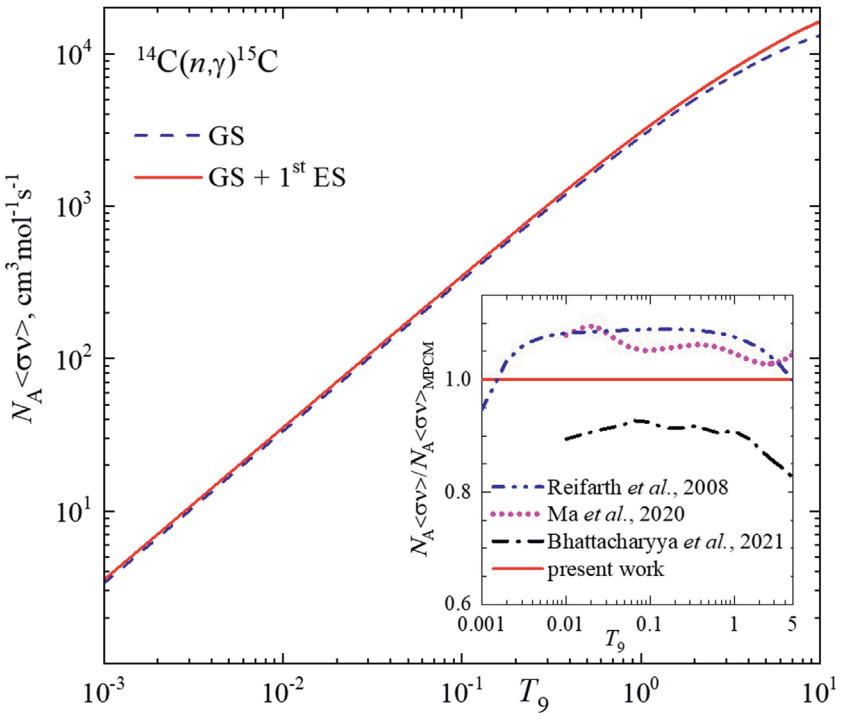

FIGURE 3
Rate of the ^{14}C(n,γ)^{15}C reaction. MPCM reaction rates: red solid curve, −GS + first ES; blue dashed curve, GS. Inset: comparison of the reaction rates from [18] (dot magenta curve), [11] (dash-dot-dot blue curve), and [19] (dash-dot black curve) normalized to the MPCM rate.

TABLE 5 Reaction rate approximation parameters for (Equation 5).

i	a_i, GS	a_i, total	i	a_i, GS	a_i, total
1	945.5511	964.222	6	−11.40699	−7.71086
2	5.09723	4.94155	7	−7.33743	−8.33403
3	−3.27812	0.29088	8	3168.048	3411.508
4	−0.26229	−16.5326	9	0.98569	0.99366
5	−32.1241	−20.09722			

In Figure 3, we do not present the results from [20] directly, but we compare our reaction rate with the tabulated data of [20]. The authors note that their rate is ~25% lower than that provided in [11] and ~2.5–4 times higher than that provided in [7]. Comparison with our rate shows that our data exceeds the rate from [20] by a factor of 1.20. We may conclude that our results are more consistent with those reported in [11, 18, 19].

5 $^{12\text{-}14}C(n,\gamma)^{13\text{-}15}C$ reaction rates and $^{12}C/^{13}C$ and $^{13}C/^{14}C$ ratios

Answer to question (i): The MPCM passed the cross-check; therefore, reliable data on the rate of the $^{14}C(n,\gamma_{0+1})^{15}C$ reaction may be considered well determined today within ~10% accuracy. This conclusion allows us to discuss possible corrections to the isotopic ratios $^{12}C/^{13}C$, $^{13}C/^{14}C$, and $^{14}N/^{15}N$, following sequence 2 by comparing the early values from Ref. [1] (Equation 1) and addressing question (ii). The first observation concerns the near factor-of-5 difference in the reaction rates reported by [7] and [8], as shown in Figure 4. This difference changes the ratio $^{13}C/^{14}C > 1400$ to $^{13}C/^{14}C > 280$. Results obtained by Wiescher et al. 25 years ago have been confirmed today.

Further changes in isotopic ratios may come from the results on reaction rates of the radiative neutron capture on carbon isotopes $^{12}C(n,\gamma)^{13}C$ [38] $^{13}C(n,\gamma)^{14}C$ [39], and $^{14}C(n,\gamma)^{15}C$ (present work) calculated in the same model—MPCM. These rates are shown in Figure 5.

Radiative neutron capture reactions may change the balance of $^{13}C/^{14}C$ as the ratio of reaction rates $R_{^{13}C/^{14}C}(T_9) = \langle\sigma v\rangle_{^{12}C(n,\gamma)^{13}C}/\langle\sigma v\rangle_{^{13}C(n,\gamma)^{14}C}$ at temperatures $T_9 = 0.01 - 0.025$ varies in the range of 2.9–3.2. These rates become equal at $T_9 \simeq 0.2$ $\left(R_{^{13}C/^{14}C} = 1\right)$, and then, up to $T_9 \simeq 1.5$, the production of ^{14}C exceeds the creation of ^{13}C ($R_{^{13}C/^{14}C} \simeq 0.5$ at $T_9 \simeq 1.1$).

Comparison of $^{13}C(n,\gamma_{0+1+2})^{14}C$ and $^{14}C(n,\gamma_{0+1})^{15}C$ rates in Figure 5 shows the temperature intervals where slow production of ^{15}C exceeds the creation of ^{14}C. The low energy interval is T_9 = 0.1–0.2, which refers to the equality of the corresponding reaction rates $\langle\sigma v\rangle_{^{13}C(n,\gamma)^{14}C} = \langle\sigma v\rangle_{^{14}C(n,\gamma)^{15}C}$ with values of ≃ 290 and ≃ 620 $cm^3mol^{-1}s^{-1}$ at the edges. At temperatures $T_9 \gtrsim 3$, the rate of ^{15}C production noticeably prevails over the rate of ^{14}C formation. It is not meaningful to discuss the unobservable ratio of $^{14}C/^{15}C$ isotopes, but the relative enhancement in the $^{14}C(n,\gamma_{0+1})^{15}C$ reaction rate may, to some extent, affect the nitrogen ratio $^{14}N/^{15}N$.

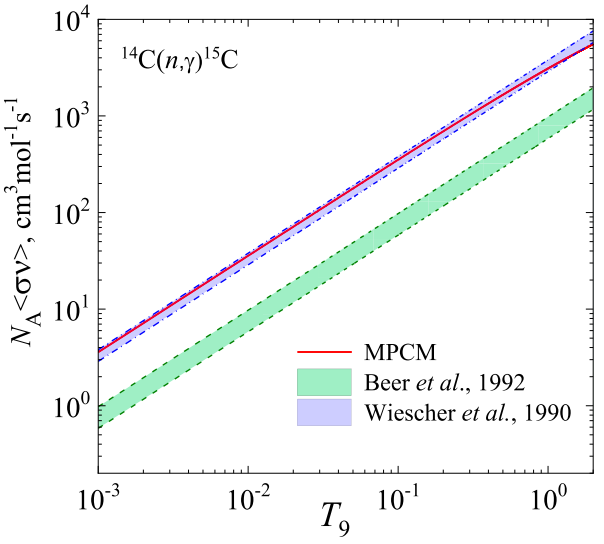

FIGURE 4
Comparison of MPCM results with the modeless calculations implemented by [7] and [8].

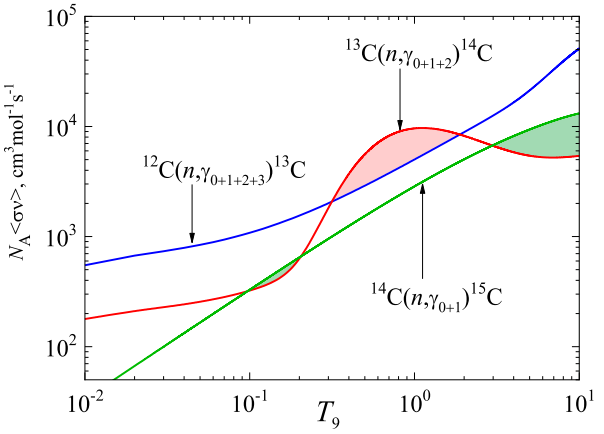

FIGURE 5
Comparison of the astrophysical $^{12}C(n,\gamma_{0+1+2+3})^{13}C$ [38], $^{13}C(n,\gamma_{0+1+2})^{14}C$ [39], and $^{14}C(n,\gamma_{0+1})^{15}C$ reaction rates in the range T_9 = 0.01–10. Colored areas correspond to the interchange of the reaction rates (see comments in text).

The production of ^{14}C in low-metallicity AGB stars is provided by two reactions: $^{13}C(n,\gamma)^{14}C$ and $^{14}N(n,p)^{14}C$ [40, 41]. Measurements by Wallner et al. [41] reported cross section at 23.3 keV $\sigma_{n,\gamma} = 6.7\,\mu b$, $\sigma_{n,p} = 1.74\,mb$, and $\sigma_{n,p}/\sigma_{n,\gamma} = 260$. The recent measurements of the Maxwellian averaged cross sections (MACS) derived from the n_TOF cross section reported the value $\sigma_{n,p}^{MACS} = 1.77 \pm 0.04\,mb$ [42] for the $kT = 25$ keV, while the data from [41] are $\sigma_{n,p}^{MACS} = 2.03 \pm 0.04\,mb$ and $\sigma_{n,\gamma}^{MACS} = 20.6 \pm 2.7\,\mu b$. Corresponding ratios $\sigma_{n,p}^{MACS}/\sigma_{n,\gamma}^{MACS}$ are 98.5 and 86, respectively. The difference in MACS between Wallner et al. [41] and Torres et.al. [41] becomes noticeable for $kT > 15$ keV and reaches a factor ~3 at $kT = 100$ keV.

In simpler terms, the ratio of these two reactions $^{13}C(n,\gamma)^{14}C$ and $^{14}N(n,p)^{14}C$ is approximately two orders of magnitude. Hence,

the relative concentrations of accumulated nuclei ^{13}C and ^{14}N set the balance between these two reactions, which provides the abundance of ^{14}C sufficient for a change in the elemental content of carbon pockets. Reaction ^{14}N$(n,p)^{14}$C changes the ratio ^{14}N/^{15}N, and at the same time, this ratio may be affected by increasing the number of ^{15}N via the reaction $^{14}\mathrm{C}(n,\gamma)^{15}\mathrm{C}(\beta^-)^{15}$N.

6 Rate of the $^{14}\mathrm{C}(n,\gamma_0)^{15}$C reaction with Tsallis statistics

It has been established that thermal pulses arise during the evolution of AGB stars and lead to temperature and density fluctuations in the convective envelope, which can locally disrupt the equilibrium particles' velocity distribution [1, 2]. The Maxwell–Boltzmann distribution may also be violated due to turbulence and sudden energetic events, such as helium and hydrogen flashes. This provides the motivation for applying Tsallis statistics [23–25], κ-distributions [43–45], and superstatistics [46] when calculating nuclear reaction rates in AGB models.

The application of Tsallis statistics is our first step toward examining non-extensive effects in stellar plasma, for example, the $^{14}\mathrm{C}(n,\gamma_0)^{15}$C reaction, which may be incorporated into the analysis of the processes occurring in the carbon pockets of AGB stars [1, 4, 6]. The reason for applying Tsallis statistics concerns several aspects. The interpretation of non-extensive parameter q in the velocity distribution $f_q(v)$ is quite straightforward; i.e., in case, $q > 1$, the Maxwell–Boltzmann $f_{\mathrm{MB}}(v)$ symmetric distribution is violated due to a damping in the number of particles with high energies, whereas case $q < 1$ implies an enhancement in the low energy component in the $f_q(v)$ distribution compared to the $f_{\mathrm{MB}}(v)$. We also find that the Tsallis formalism is rather simple in application for calculating reaction rate integrals as it allows for convergent control of the results to those of the Maxwell–Boltzmann distribution.

Following [24] and [25], we recalculated the rate of the $^{14}\mathrm{C}(n,\gamma)^{15}$C reaction simulating the non-extensive effect of Tsallis statistics versus the Maxwell–Boltzmann by changing the velocity distribution from $f_{\mathrm{MB}}(v)$ to $f_q(v)$. Explicit expressions and normalizing conditions for the velocity distributions of non-relativistic particles with an energy $E = \mu v^2/2$ in the center-of-mass system are

$$f_{MB}(v) = 4\pi\left(\frac{\mu}{2\pi kT}\right)^{3/2} e^{-\frac{\mu v^2}{2kT}} v^2, \int_0^\infty f_{MB}(v)\,dv = 1, \tag{6}$$

$$f_q(v) = B_q 4\pi\left(\frac{\mu}{2\pi kT}\right)^{\frac{3}{2}}\left[1-(q-1)\frac{\mu v^2}{2kT}\right]^{\frac{1}{q-1}} v^2, \int f_q(q)dv = 1. \tag{7}$$

Note that $\lim_{q\to 1}\left[1-(q-1)\frac{E}{kT}\right]^{\frac{1}{q-1}} = e^{-\frac{E}{kT}}$, so the case $q = 1$ of the non-extensive parameter refers to the MB velocity distribution. Normalizing condition in Equation 7 allows us to calculate analytically the normalizing constants B_q and express them via the gamma-function $\Gamma(z)$:

$$B_q = (1-q)^{3/2}\frac{\Gamma\left(\frac{1}{1-q}\right)}{\Gamma\left(\frac{1}{1-q}-\frac{3}{2}\right)}, \quad \text{if} \quad \frac{1}{3} \le q < 1, \tag{8}$$

TABLE 6 Normalizing constants B_q and values of $E_{\max}$ (for $q > 1$).

$q > 1$	B_q	$E_{\max}$, MeV	$q < 1$	B_q
1.01	1.018801	8.6173	0.99	0.981301
1.05	1.095010	1.7235	0.95	0.907529
1.10	1.192506	0.8617	0.90	0.817653
1.30	1.606347	0.2872	0.70	0.485298

$$B_q = (q-1)^{3/2}\left(\frac{1}{q-1}+\frac{3}{2}\right)\left(\frac{1}{q-1}+\frac{1}{2}\right)\frac{\Gamma\left(\frac{1}{q-1}+\frac{1}{2}\right)}{\Gamma\left(\frac{1}{q-1}+1\right)}, \quad \text{if } q > 1. \tag{9}$$

In the case of $q < 1$, there is no limit of particles by the energy, i.e., $E_{\max} = \infty$. In the case of $q > 1$, the kinetic energy is limited as $E_{\max} = \frac{kT}{q-1}$, $kT = 0.086173 \cdot T_9$ (MeV). In Table 6, a few values of B_q (Equations 8, 9) and $E_{\max}$ are presented.

The integral over the Maxwellian-weighted cross section (Equation 6) determines the reaction rate, which was derived in detail by Iliadis and is provided in a general form [47]:

$$N_A\langle\sigma v\rangle = N_A\left(\frac{8}{\pi\mu}\right)^{1/2}(kT)^{-3/2}\int_0^\infty \sigma(E)E\exp\left(-\frac{E}{kT}\right)dE. \tag{10}$$

Equation 10 along with substituted numerical values for the constants is expressed as:

$$N_A\langle\sigma v\rangle_{\mathrm{MB}} = 3.7313\cdot 10^4\mu^{-1/2}T_9^{-3/2}\int_0^\infty \sigma(E)E\exp\left(-11.605E/T_9\right)dE. \tag{11}$$

In the case of Tsallis statistics and following definition for $f_q(v)$ distribution (Equation 7), Equation 11 can be transformed to

$$N_A\langle\sigma v\rangle_q = B_q\cdot 3.7313\cdot 10^4\mu^{-1/2}T_9^{-3/2}\int_0^{E_{\max}} \sigma(E)E\left[1-(q-1)\cdot 11.605E/T_9\right]^{\frac{1}{q-1}}dE. \tag{12}$$

In Figure 6 the results of the calculated $\langle\sigma v\rangle_q$ reaction rate of the radiative neutron capture to the GS of the ^{15}C nucleus for the interval of non-extensive parameter $0.7 \le q \le 1.3$ are presented. It is clear that the case $q > 1$ corresponds to the inequality $\langle\sigma v\rangle_q < \langle\sigma v\rangle_{\mathrm{MB}}$, which can be explained by looking at the $E_{\max}$ values of q in Table 6 and the energy dependence of the total cross section $\sigma(E)$ in Figure 1. Since no cut-off of integrand in Equation 12 in the case of $q < 1$, the corresponding reaction rates are related as $\langle\sigma v\rangle_q > \langle\sigma v\rangle_{\mathrm{MB}}$.

Figure 7 shows the numerical difference in reaction rates, considering the effect of the non-equilibrium Tsallis distribution compared to the MB distribution for $0.9 \le q \le 1.1$. The difference in rates $\langle\sigma v\rangle_q/\langle\sigma v\rangle_{\mathrm{MB}}$ is ~4%–35% increase for $0.99 \le q \le 1.1$ and ~4–20% decrease for $1.01 \le q \le 1.10$. Figure 6 shows a factor ~4 increase in $\langle\sigma v\rangle_q$ for $q = 0.7$ and a factor ~0.6 decrease for $q = 1.3$.

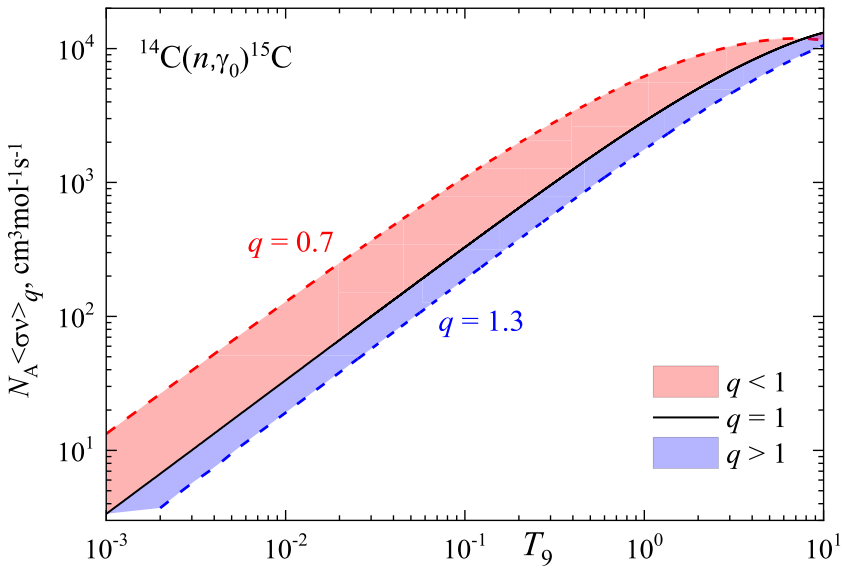

FIGURE 6
Reaction rates calculated for the Tsallis statistics: $q > 1$ – blue band, $q < 1$ – red band relative to the Maxwellian-Boltzmann rate–black solid curve.

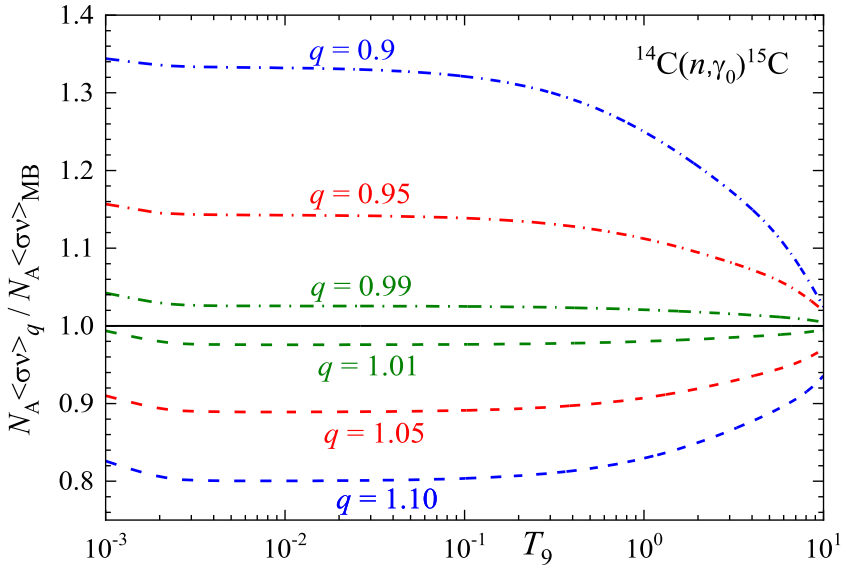

FIGURE 7
Ratio of the Tsallis reaction rates to the Maxwell–Boltzmann rate.

In [20] Jiang et al., implemented the calculated $^{14}C(n,\gamma)^{15}C$ reaction rate $\langle\sigma v\rangle_{MB}$ for the estimation of the ^{15}N abundance, which results in ~20% increase of nitrogen-15 production, but only ~0.2% impact on the final abundances of heavy elements with $A > 90$. As we mentioned above, the present $\langle\sigma v\rangle_{MB}$ rate for this reaction is ~1.2 times higher than reported in [20]. If we assume the non-extensive parameter $q = 0.7$, the increasing factor for the reaction rate $\langle\sigma v\rangle_q$ is ~5; therefore, ^{15}N abundance may increase much higher than estimations based on the rate by Jiang et al., 2025. Note that the value $q = 0.7$ refers to a rather strong enhancement of the high-energy tails, which may arise from extreme events in the AGB environment.

Note that we have implemented a simplified calculation procedure, assuming that the effect of the center-of-mass correction, introduced by [26, 27], is not essential, as the seed nucleus ^{14}C is much heavier than the light species with comparable masses involved at the stage of primordial BBN.

7 Conclusion

In summary, we show that the MPCM results on $^{14}C(n,\gamma_{0+1})^{15}C$ are in good agreement with those reported in [18, 19]. Benchmark

cross section σ(23.3keV) = 4.75 μb matches the presently recommended value 4.86(48) μb reported in [18]. The Maxwellian-weighted reaction rates calculated in the MPCM agree within ~±10% deviations with the independent calculations of [8, 11, 18], and [19], therefore, the data on the MB rate of the ^{14}C(n,γ)^{15}C reaction can be considered well determined today.

The obtained values of reaction rates can be confidently conceived as the reference ones for the re-estimation of ^{12}C/^{13}C, ^{13}C/^{14}C, and ^{14}N/^{15}N via the neutron-induced reactions ^{12}C(n,$\gamma_{0+1+2+3}$)^{13}C, ^{13}C(n,γ_{0+1+2})^{14}C, and ^{14}C(n,γ_{0+1})^{15}C calculated in MPCM. We determined the temperature windows where the interchange of reaction rates is observed: $\langle\sigma v\rangle_{^{13}C(n,\gamma)^{14}C} > \langle\sigma v\rangle_{^{12}C(n,\gamma)^{13}C}$ at T_9 = 0.2–1.5; $\langle\sigma v\rangle_{^{14}C(n,\gamma)^{15}C} > \langle\sigma v\rangle_{^{13}C(n,\gamma)^{14}C}$ at AGB stars' actual temperatures T_9 = 0.1–0.2 and at higher values $T_9 \gtrsim 3$.

Here, in order to finalize the values of isotopic ratios, it is reasonable to consider the reaction rates $^{12\text{-}14}$C(n,γ)$^{13\text{-}15}$C together with the proton-induced reactions $^{12\text{-}14}$C(p,γ)$^{13\text{-}15}$N calculated in the same model. We took a step forward toward this goal by calculating the MPCM rate for the ^{12}C(p,γ)^{13}N reaction [48].

The Tsallis statistics allow one to vary the numerical values of the ^{14}C(n,γ_{0+1})^{15}C reaction rate, as illustrated in the present calculations for the range of the non-extensive parameter $0.7 \leq q \leq 1.3$. This provides a tool for the re-estimation of astrophysical processes occurring in low-metallicity AGB stars, in particular, the production and depletion carbon isotopes as reflected in the observed ^{13}C/^{14}C ratio. Note that the value of the ^{13}C/^{14}C ratio directly affects the ratio of nitrogen isotope yields, ^{14}N/^{15}N. Comparing these results with studies of BBN reactions [25–27], the effect of non-extensivity in the case of the ^{14}C(n,γ_0)^{15}C reaction is moderate—not orders of magnitude—but can produce a maximum factor of ~1.35 increase or ~0.8 decrease in the MB reaction rate for $0.9 \leq q \leq 1.1$. One reason for this moderate effect may be that, in the case of BBN, charged particles of comparable mass are involved in the reactions.

Data availability statement

The original contributions presented in the study are included in the article/supplementary material, further inquiries can be directed to the corresponding author.

Author contributions

AT: Conceptualization, Supervision, Writing – review and editing. NB: Formal analysis, Writing – original draft. BY: Data curation, Writing – review and editing. SD: Software, Validation, Writing – review and editing.

Funding

The author(s) declare that financial support was received for the research and/or publication of this article. This work was supported by the Ministry of Science and Higher Education of the Republic of Kazakhstan (Grant No. AP19676483).

Conflict of interest

The authors declare that the research was conducted in the absence of any commercial or financial relationships that could be construed as a potential conflict of interest.

Generative AI statement

The author(s) declare that no Generative AI was used in the creation of this manuscript.

Any alternative text (alt text) provided alongside figures in this article has been generated by Frontiers with the support of artificial intelligence and reasonable efforts have been made to ensure accuracy, including review by the authors wherever possible. If you identify any issues, please contact us.

Publisher's note

References

1. Forestini M, Charbonnel C. Nucleosynthesis of light elements inside thermally pulsing AGB stars. *Astron Astrophys Suppl Ser* (1997) 123:241–72. doi:10.1051/aas:1997348

2. Forestini M, Guelin M, Cernicharo J. ^{14}C in AGB stars: the case of IRC+10216. *Astron Astrophys* (1997) 317:883–8.

3. Karakas AI, Lattanzio JC. The dawes review 2: nucleosynthesis and stellar yields of Low- and intermediate-mass single stars. *Publ Astron Soc Aust* 31:e030. (2014) doi:10.1017/pasa.2014.21

4. Palmerini S, Busso M, Vescovi D, Naselli E, Pidatella A, Mucciola R, et al. Presolar grain isotopic ratios as constraints to nuclear and stellar parameters of asymptotic giant branch star nucleosynthesis. *Astrophys J* (2021) 921:7. doi:10.3847/1538-4357/ac1786

5. Herwig F. Evolution of asymptotic giant branch stars. *Annu Rev Astron Astrophys* (2005) 43:435–79. doi:10.1146/annurev.astro.43.072103.150600

6. Choplin A, Siess L, Goriely S. Proton ingestion in asymptotic giant branch stars as a possible explanation for J-type stars and AB2 grains. *Astron Astrophys* (2024) 691:L7. doi:10.1051/0004-6361/202451013

7. Beer H, Wiescher M, Kaeppeler F, Goerres J, Koehler PE. A measurement of the C-14(n, gamma)C-15 cross section at a stellar temperature of kT = 23.3 keV. *Astrophys J* (1992) 387:258. doi:10.1086/171077

8. Wiescher M, Gorres J, Thielemann F-K. Capture reactions on C-14 in nonstandard big bang nucleosynthesis. *Astrophys J* (1990) 363:340. doi:10.1086/169348

9. Horvath A, Weiner J, Galonsky A, Deak F, Higurashi Y, Ieki K, et al. Cross section for the astrophysical ^{14}C(n,γ)^{15}C reaction via the inverse reaction. *Astrophys J* (2002) 570:926–33. doi:10.1086/339726

10. Reifarth R, Heil M, Plag R, Besserer U, Dababneh S, Dörr L, et al. Stellar neutron capture rates of ^{14}C. *Nucl Phys A* (2005) 758:787–90. doi:10.1016/j.nuclphysa.2005.05.141

11. Reifarth R, Heil M, Forssén C, Besserer U, Couture A, Dababneh S, et al. The $^{14}C(n,\gamma)$ cross section between 10 keV and 1 MeV. *Phys Rev C* (2008) 77:015804. doi:10.1103/PhysRevC.77.015804

12. Nakamura T, Fukuda N, Aoi N, Imai N, Ishihara M, Iwasaki H, et al. Neutron capture cross section of ^{14}C of astrophysical interest studied by coulomb breakup of ^{15}C. *Phys Rev C* (2009) 79:035805. doi:10.1103/PhysRevC.79.035805

13. Timofeyuk NK, Baye D, Descouvemont P, Kamouni R, Thompson IJ. ^{15}C–^{15}F charge symmetry and the $^{14}C(n,\gamma)^{15}C$ reaction puzzle. *Phys Rev Lett* (2006) 96:162501. doi:10.1103/PhysRevLett.96.162501

14. Summers NC, Nunes FM. Extracting (n,γ) direct capture cross sections from coulomb dissociation: application to $^{14}C(n,\gamma)^{15}C$. *Phys Rev C* (2008) 78:011601. doi:10.1103/PhysRevC.78.011601

15. McCleskey M, Mukhamedzhanov AM, Trache L, Tribble RE, Banu A, Eremenko V, et al. Determination of the asymptotic normalization coefficients for $^{14}C + n \leftrightarrow {}^{15}C$, the $^{14}C(n,\gamma)^{15}C$ reaction rate, and evaluation of a new method to determine spectroscopic factors. *Phys Rev C* (2014) 89:044605. doi:10.1103/PhysRevC.89.044605

16. Capel P, Nollet Y. Reconciling coulomb breakup and neutron radiative capture. *Phys Rev C* (2017) 96:015801. doi:10.1103/PhysRevC.96.015801

17. Moschini L, Yang J, Capel P. ^{15}C: from halo effective field theory structure to the study of transfer, breakup, and radiative-capture reactions. *Phys Rev C* (2019) 100:044615. doi:10.1103/PhysRevC.100.044615

18. Ma T, Guo B, Pang D, Li Z, Su Y, Li X, et al. New determination of astrophysical $^{14}C(n, \gamma)^{15}C$ reaction rate from the spectroscopic factor of ^{15}C. *Sci China Phys Mech Astron* (2020) 63:212021. doi:10.1007/s11433-019-9411-2

19. Bhattacharyya A, Datta U, Rahaman A, Chakraborty S, Aumann T, Beceiro-Novo S, et al. Neutron capture cross sections of light neutron-rich nuclei relevant for *r*-process nucleosynthesis. *Phys Rev C* (2021) 104:045801. doi:10.1103/PhysRevC.104.045801

20. Jiang Y, He Z, Luo Y, Xin W, Chen J, Li X, et al. New determination of the $^{14}C(n,\gamma)^{15}C$ reaction rate and its astrophysical implications. *Astrophys J* (2025) 989:231. doi:10.3847/1538-4357/ade5b3

21. Dubovichenko SB, Uzikov YN. Astrophysical *S*-factors of reactions with light nuclei. *Phys Particles Nuclei* (2011) 42:251–301. doi:10.1134/S1063779611020031

22. Dubovichenko SB. *Radiative neutron capture: primordial nucleosynthesis of the universe*. Berlin: De Gruyter (2019).

23. Tsallis C. Possible generalization of boltzmann-gibbs statistics. *J Stat Phys* (1988) 52:479–87. doi:10.1007/BF01016429

24. Hou SQ, He JJ, Parikh A, Daid K, Bertulani C. Big-bang nucleosynthesis verifies classical maxwell-boltzmann distribution (2014) Available online at: http://arxiv.org/abs/1408.4422 (Accessed Feburary 07, 2025).

25. Hou SQ, He JJ, Parikh A, Kahl D, Bertulani CA, Kajino T, et al. Non-extensive statistics to the cosmological lithium problem. *Astrophys J* (2017) 834:165. doi:10.3847/1538-4357/834/2/165

26. Kusakabe M, Kajino T, Mathews GJ, Luo Y. On the relative velocity distribution for general statistics and an application to big-bang nucleosynthesis under tsallis statistics. *Phys Rev D* (2019) 99:043505. doi:10.1103/PhysRevD.99.043505

27. Bertulani CA. Shubhchintak. Primordial nucleosynthesis with non-extensive statistics. *Eur Phys J Spec Top* (2024) 233:2831–42. doi:10.1140/epjs/s11734-024-01216-0

28. Dubovichenko S, Dzhazairov-Kakhramanov A, Afanasyeva N. Radiative neutron capture on ^{9}Be, ^{14}C, ^{14}N, ^{15}N and ^{16}O at thermal and astrophysical energies. *Int J Mod Phys E* (2013) 22:1350075. doi:10.1142/S0218301313500754

29. Mukhamedzhanov AM, Tribble RE. Connection between asymptotic normalization coefficients, subthreshold bound states, and resonances. *Phys Rev C* (1999) 59:3418–24. doi:10.1103/PhysRevC.59.3418

30. Yamaguchi T, Hachiuma I, Kitagawa A, Namihira K, Sato S, Suzuki T, et al. Scaling of charge-changing interaction cross sections and point-proton radii of neutron-rich carbon isotopes. *Phys Rev Lett* (2011) 107:032502. doi:10.1103/PhysRevLett.107.032502

31. Zhao JW, Sun B-H, Tanihata I, Xu JY, Zhang KY, Prochazka A, et al. Charge radii of $^{11-16}C$, $^{13-17}N$ and $^{15-18}O$ determined from their charge-changing cross-sections and the mirror-difference charge radii. *Phys Lett B* (2024) 858:139082. doi:10.1016/j.physletb.2024.139082

32. Zhao JW, Sun B-H, Tanihata I, Terashima S, Prochazka A, Xu JY, et al. Isospin-dependence of the charge-changing cross-section shaped by the charged-particle evaporation process. *Phys Lett B* (2023) 847:138269. doi:10.1016/j.physletb.2023.138269

33. Li LY, Tu XL, Zhang JT, Zhang GQ. Nuclear matter distribution radius compilation and evaluation: NMRCE2025. *At Data Nucl Data Tables* (2025) 166:101747. doi:10.1016/j.adt.2025.101747

34. Kanungo R, Horiuchi W, Hagen G, Jansen GR, Navratil P, Ameil F, et al. Proton distribution radii of $^{12\text{-}19}C$ illuminate features of neutron halos. *Phys Rev Lett* (2016) 117:102501. doi:10.1103/PhysRevLett.117.102501

35. Dobrovolsky AV, Korolev GA, Tang S, Alkhazov GD, Colò G, Dillmann I, et al. Nuclear matter distributions in the neutron-rich carbon isotopes $^{14-17}C$ from intermediate-energy proton elastic scattering in inverse kinematics. *Nucl Phys A* (2021) 1008:122154. doi:10.1016/j.nuclphysa.2021.122154

36. Hebborn C, Capel P. Halo effective field theory analysis of one-neutron knockout reactions of ^{11}Be and ^{15}C. *Phys Rev C* (2021) 104:024616. doi:10.1103/PhysRevC.104.024616

37. Ajzenberg-Selove F. Energy levels of light nuclei A = 13–15. *Nucl Phys A* (1991) 523:1–196. doi:10.1016/0375-9474(91)90446-D

38. Dubovichenko SB, Burkova NA. Rate of radiative $n^{12}C$ decay at temperatures from 0.01 T_9 to 10 T_9. *Russ Phys J* (2021) 64:216–27. doi:10.1007/s11182-021-02319-0

39. Dubovichenko SB. $n^{13}C$ capture reaction rate. *Russ Phys J* (2022) 65:208–15. doi:10.1007/s11182-022-02624-2

40. Lugaro M, Herwig F, Lattanzio JC, Gallino R, Straniero O. Process nucleosynthesis in asymptotic giant branch stars: a test for stellar evolution. *Astrophys J* (2003) 586:1305–19. doi:10.1086/367887

41. Wallner A, Bichler M, Buczak K, Dillmann I, Käppeler F, Karakas A, et al. Accelerator mass spectrometry measurements of the $^{13}C(n,\gamma)^{14}C$ and $^{14}N(n,p)^{14}C$ cross sections. *Phys Rev C* (2016) 93:045803. doi:10.1103/PhysRevC.93.045803

42. Torres-Sánchez P, Praena J, Porras I, Sabaté-Gilarte M, Lederer-Woods C, Aberle O, et al. Measurement of the $^{14}N(n,p)^{14}C$ cross section at the CERN n_TOF facility from subthermal energy to 800 keV. *Phys Rev C* (2023) 107:064617. doi:10.1103/PhysRevC.107.064617

43. Kong H, Xie H, Liu B, Tan M, Luo D, Li Z, et al. Enhancement of fusion reactivity under Non-Maxwellian distributions: effects of drift-ring-beam, slowing-down, and kappa super-thermal distributions. *Plasma Phys Control Fusion* (2024) 66:015009. doi:10.1088/1361-6587/ad1008

44. Squarer BI, Presilla C, Onofrio R. Enhancement of fusion reactivities using Non-Maxwellian energy distributions. *Phys Rev E* (2024) 109:025207. doi:10.1103/PhysRevE.109.025207

45. Livadiotis G. Kappa distributions: statistical physics and thermodynamics of space and astrophysical plasmas. *Universe* (2018) 4:144. doi:10.3390/universe4120144

46. Ourabah K. Reaction rates in quasiequilibrium states. *Phys Rev E* (2025) 111:034115. doi:10.1103/PhysRevE.111.034115

47. Iliadis C. *Nuclear physics of stars*. Second. Weinheim, Germany: Wiley-VCH Verlag GmbH and Co. KGaA (2015).

48. Dubovichenko SB, Burkova NA, Tkachenko AS, Samratova A. Reaction rate of radiative $p^{12}C$ capture in a modified potential cluster model. *Chin Phys C* (2025) 49:044104. doi:10.1088/1674-1137/ada34d

49. Mukhamedzhanov AM, Burjan V, Gulino M, Hons V, Kroha Z, McCleskey M, et al. Asymptotic normalization coefficients from the $^{14}C(d,p)^{15}C$ reaction. *Phys. Rev. C* (2011) 84:024616. doi:10.1103/PhysRevC.84.024616